Analyst

ROYAL SOCIETY OF CHEMISTRY

PAPER

View Article Online
View Journal | View Issue

Check for updates

Cite this: *Analyst*, 2021, **146**, 1772

Nuclear hyperpolarization of (1-^{13}C)-pyruvate in aqueous solution by proton-relayed side-arm hydrogenation†

Laurynas Dagys,[a] Anil P. Jagtap,[b,c] Sergey Korchak,[b,c] Salvatore Mamone,[b,c] Philip Saul,[b,c] Malcolm H. Levitt *[a] and Stefan Glöggler *[b,c]

Received 15th December 2020,
Accepted 15th January 2021

DOI: 10.1039/d0an02389b

rsc.li/analyst

We employ Parahydrogen Induced Polarization with Side-Arm Hydrogenation (PHIP-SAH) to polarize (1-^{13}C)-pyruvate. We introduce a new method called proton-relayed side-arm hydrogenation (PR-SAH) in which an intermediate proton is used to transfer polarization from the side-arm to the ^{13}C-labelled site of the pyruvate before hydrolysis. This significantly reduces the cost and effort needed to prepare the precursor for radio-frequency transfer experiments while still maintaining acceptable polarization transfer efficiency. Experimentally we have attained on average 4.33% ^{13}C polarization in an aqueous solution of (1-^{13}C)-pyruvate after about 10 seconds of cleavage and extraction. PR-SAH is a promising pulsed NMR method for hyperpolarizing ^{13}C-labelled metabolites in solution, conducted entirely in high magnetic field.

Open Access Article. Published on 15 January 2021. Downloaded on 2/20/2026 8:36:43 PM.
This article is licensed under a Creative Commons Attribution 3.0 Unported Licence.

1. Introduction

Hyperpolarization methods are a group of techniques that address the limited sensitivity of Nuclear Magnetic Resonance (NMR).[1–9] These methods have led to promising progress towards highly polarized molecules for use in the chemical and biological sciences as molecular imaging agents[8,10,11] some of which are already on their way to clinical diagnostics.[12–14] Among the several metabolic substrates that have been hyperpolarized, (1-^{13}C)-pyruvate is, by far, the most widely investigated.[15,16] Pyruvate participates in several important metabolic processes, such as glycolysis, which makes it a compelling probe of energy metabolism in biological systems.[12–17]

One of the fastest hyperpolarization methods is parahydrogen-induced polarization (PHIP).[2,3,7,17–31] It has a number of advantages, such as its low-cost, compact and easy application without the need of dedicated cryo-cooled high-field magnets, and the ability to produce large quantities of polarized material on demand. The method uses spin order from the *para*-spin isomer of molecular hydrogen which is provided by chemical interactions between a substrate of interest, solvent and a catalyst.[3,32]

One of the most effective ways to hyperpolarize pyruvate with parahydrogen is the side-arm hydrogenation (SAH) procedure (Fig. 1).[23–25] In PHIP-SAH, a ^{13}C-labeled metabolite is attached to a side-arm with an unsaturated bond. This side-arm is subsequently hydrogenated in an organic solvent with *para*-enriched hydrogen resulting in high nuclear spin order. The order is transferred from the side-arm protons to the ^{13}C of the target molecule by a variety of methods, as discussed

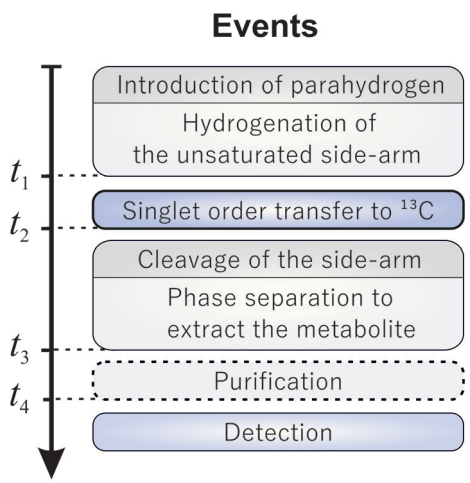

Fig. 1 Generalized PHIP-SAH timing scheme. The indicated time points are related to the procedure depicted in Fig. 2.

[a]*School of chemistry, Highfield Campus, Southampton, SO171BJ, UK. E-mail: mhl@soton.ac.uk*
[b]*Max Planck Inst. Biophys. Chem., NMR Signal Enhancement Grp., Am Fassberg 11, D-37077 Göttingen, Germany. E-mail: stefan.gloeggler@mpibpc.mpg.de*
[c]*Center for Biostructural Imaging of Neurodegeneration of UMG, Von-Siebold-Str. 3A, D-37075 Göttingen, Germany*

†Electronic supplementary information (ESI) available. See DOI: 10.1039/D0AN02389B

This journal is © The Royal Society of Chemistry 2021

Open Access Article. Published on 15 January 2021. Downloaded on 2/20/2026 8:36:43 PM.
This article is licensed under a Creative Commons Attribution 3.0 Unported Licence.

below. After achieving strong ^{13}C magnetization, the side-arm is cleaved off with an aqueous basic solution, thereby extracting the desired hyperpolarized metabolite into the aqueous phase.[23] For biological uses, the pH of the obtained solution is adjusted as the last step.

The achievable ^{13}C magnetization yield is dictated by the achievable proton spin order, the polarization transfer step, and relaxation losses during the chemical reactions and pulse sequence. The most common way to perform the transfer step is to use field cycling techniques achieving about 5% ^{13}C polarization of pyruvate enriched in the 1-^{13}C position.[16,33–39] This involves changing the magnetic field from earth to near zero field which converts the initial spin-order into ^{13}C magnetization. However, the use of the low-field regime normally requires 1 m or more of separation between the site of spin order conversion and the site of the NMR or MRI experiment for metabolic studies (normally inside the bore of a high-field magnet).

Methods have been proposed in which the spin order transformation step is conducted entirely in high magnetic fields using radiofrequency pulse sequences.[40–44] This is particularly useful for *in vivo* applications since it allows the polarization to be conducted in close proximity to the organism under study. Hence, polarization losses are minimized. Such a realization was recently demonstrated *via* the SAMBADENA (Synthesis Amid the Magnet Bore Allows Dramatically Enhanced Nuclear Alignment) approach and was so far shown for the xenobiotic hydroxyethyl propionate only.[42,43] A first study to hyperpolarize pyruvate using pulsed PHIP-SAH required the use of two ^{13}C sites, one located in the sidearm and one located in the target metabolite.[40] After hydrogenation of the molecule the spin order is relayed *via* the sidearm-^{13}C to the ^{13}C of interest and cleavage yields the free metabolite. For free (1-^{13}C)pyruvate 3.4% polarization was so far achieved. However, the cleavage experiments were only performed in organic solvents and no extraction into the aqueous phase was demonstrated.[40]

We introduce a new method called proton-relayed sidearm hydrogenation (PR-SAH), in which a bridging hydrogen nucleus is used instead of an additional ^{13}C-labelled site, reducing the cost and effort of isotopic labelling with respect to rf-transfer methods. We also demonstrate that extraction of the hyperpolarized metabolite into an aqueous phase is possible without unacceptable loss of polarization.

The proposed molecular system for side-arm hydrogenation experiments is shown in Fig. 2(a). The new side arm (3-butyn-2-ol-d$_5$) consists of a terminal triple bond, one proton for the relay and is otherwise deuterated. The sidearm is attached to the 1-^{13}C-pyruvate moiety by a cleavable ester linkage. Addition of the *para*-enriched hydrogen (parahydrogen) to the unsaturated side-arm of the molecule **I** as shown in Fig. 2(a), deposits the singlet order of the parahydrogen between two, now vicinal, protons.

The singlet nuclear spin order from the *para*-enriched hydrogen is first transferred to the "relay" proton, and then on to the pyruvate-^{13}C, as shown in Fig. 2(b). These steps are performed by the radiofrequency pulse sequence discussed in this article. The polarized metabolite is released from the side-arm by a rapid injection of sodium hydroxide (Fig. 2(c)). The free pyruvate is dissolved into deuterated water whereas the catalyst stays in the organic phase. This also acts as an extraction step since the organic and aqueous phases separate, leaving highly polarized pyruvate dissolved in water. This finalizes all steps up to t_3 marked in the general scheme (Fig. 1) and takes around 19 s in total. Our experiments show that after the polarization transfer (but before cleavage) 7.1% ^{13}C polarization is obtained at the site of interest. After cleavage and phase extraction we achieved 4.3% ^{13}C polarization of 1 mM pyruvate in the aqueous phase. Thus, PR-SAH could be a potentially useful cost-effective approach to perform hyperpolarized ^{13}C experiments entirely in high field.

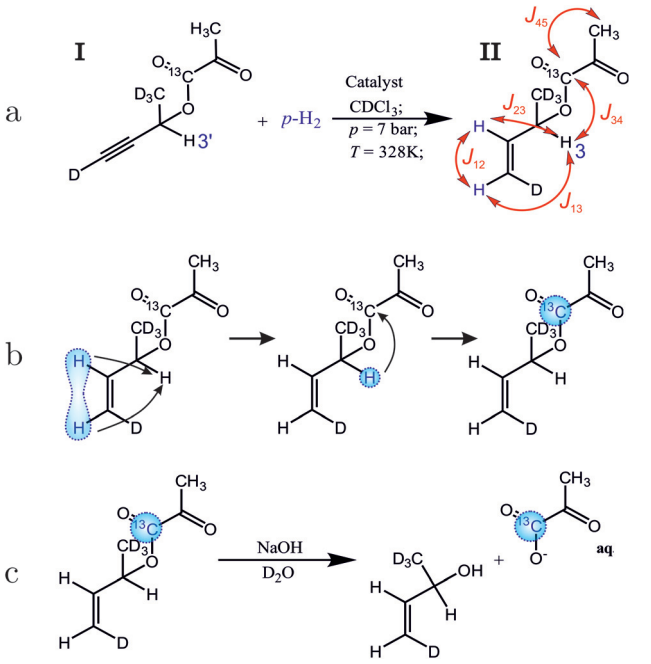

Fig. 2 Proton-relayed side-arm hydrogenation (PR-SAH) scheme. (a) Hydrogenation of the precursor molecule **I** with parahydrogen to form the hyperpolarized molecule **II**. Red symbols and arrows represent J couplings between spins of interest: $|J_{12}|$ = 10.6 Hz, $|J_{23}|$ = 6.2 Hz, $|J_{13}|$ = ~1 Hz, $|J_{34}|$ = 2.9 Hz, $|J_{45}|$ = 1.5 Hz. The chemical shifts of the protons of interest are as follows: (1) 5.20 ppm, (2) 5.88 ppm, (3) 5.44 ppm, (3′) 5.50 ppm. (b) Spin-order transfer from the former parahydrogen protons to the ^{13}C of the pyruvate, *via* the relaying proton. (c) Cleavage reaction to detach the highly polarized pyruvate from the side-arm using a basic solution.

2. Methods

2.1. Materials

The precursor molecule **I** was synthesised in three steps including esterification of the side-arm 3-butyn-2-ol-d$_5$ and (1-^{13}C)pyruvic acid. The detailed synthesis and validation of the precursor compound can be found in ESI.† The catalyst

Open Access Article. Published on 15 January 2021. Downloaded on 2/20/2026 8:36:43 PM.
This article is licensed under a Creative Commons Attribution 3.0 Unported Licence.

[Rh(dppb)(COD)]BF_4 (CAS Number 79255-71-3) was purchased from Sigma Aldrich. Other materials such as choloform-d_1, ethanol-d_1 and D_2O were also provided by the same vendor.

para-Enriched hydrogen was continuously produced by a Bruker parahydrogen generator (BPHG90), with a specified parahydrogen content of 82%. The hydrogen gas was pressurized to 10 bar.

The cleavage solution consisted of 150 mM sodium hydroxide dissolved in D_2O.

2.2. Equipment

The hyperpolarization setup consists of a 5 mm NMR tube inside a cryomagnet to which 7 bar gauge pressure of parahydrogen is delivered. A plastic tubing and a thin glass capillary reaching to the bottom of the tube supplied the *para*-enriched hydrogen to the reaction mixture. The flow of the gas was controlled by magnetic valves located in close vicinity to the cryomagnet. The valves are driven by amplified electronic pulses from the NMR spectrometer triggered *via* the pulse program. The setup facilitated all of the following PHIP experiments.

Experiments were conducted on a Bruker Avance AVANCE III HD spectrometer coupled with a 300 MHz Bruker Ascend magnet equipped with a 5 mm BBO probe. The excitation pulses were set to ~26.5 kHz and ~33.3 kHz nutation frequency for ^{1}H and ^{13}C respectively. All ^{1}H pulses used an irradiation frequency corresponding to the chemical shift of 5.90 ppm, except for one selective pulse, which used a ^{1}H irradiation frequency corresponding to 5.44 ppm, in order to match an individual alkene ^{1}H resonance (see below). The shape of the selective pulse consisted of 1000 points approximating a 14.7 ms long Gaussian pulse with a truncation at 1% of the total height. The ^{13}C spectra were collected with 256k real-data point density for 250 ppm width. Resonant ^{2}H irradiation was applied throughout all experiments to decouple ^{2}H from the rest of the spin system.

3. Proton-relayed side-arm hydrogenation

3.1. Sample preparation and hydrogenation

The synthesized precursor but-3-yn-2-yl-1,1,1,4-d_4 2-oxopropanoate-1-^{13}C (molecule **I**) and the catalyst were added into a small glass vial. The chloroform-d_1 solvent was added and the mixture was sonicated for several minutes. The default 2 mL stock solution contained 5 mM of the catalyst and ~2.5 mM of the precursor molecule. The cleavage experiments required the solvent to be a 9 : 1 mix of chloroform-d_1 and ethanol-d_1.

Prior to NMR experiments, the NMR tube was filled with a 150 μL aliquot of the stock solution. The solution was deoxygenated with nitrogen gas for 1 minute, inserted into the magnet and the temperature equilibrated at 55 °C.

The sample was pressurized with parahydrogen for 2 seconds and bubbled for 5 seconds. A 1 second delay was allowed for the bubbles to dissipate before the application of resonant rf pulses.

The side-arm hydrogenation experiments were repeated three times in order to assess the reproducibility of the procedure and to assess the standard deviation of the resulting polarization.

3.2. Polarization transfer

The polarization transfer sequence is shown in Fig. 3 and is a modified version of the ESOTHERIC (Efficient Spin Order Transfer to HEteronuclei with Relayed INEPT Chains) scheme containing 3 consecutive INEPT blocks.[40,41,44] The pulse sequence operates under weak coupling conditions, which is fulfilled due to the large chemical shift differences between all of the coupled ^{1}H spins with respect to their *J*-coupling. The exact timings of the sequence seen in Fig. 3 are τ_1 = 74.62 ms, τ_2 = 22.6 ms, τ_3 = 24.6 ms, τ_4 = 350 ms unless stated otherwise.

We treat molecule **II** as 4-spin system throughout the article ignoring the deuterons and the remote methyl protons of the

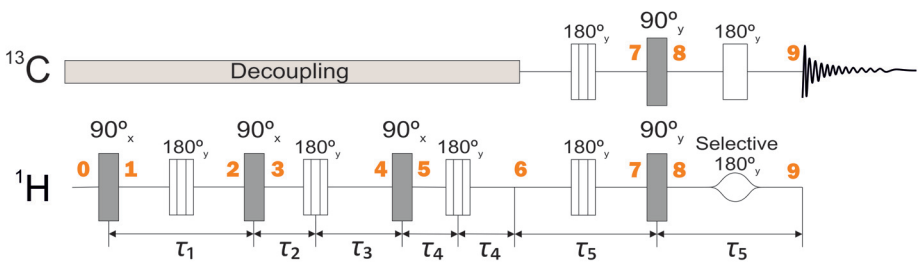

$\rho_0 = 2I_{1z}I_{2z}$ $\rho_1 = -2I_{1y}I_{2y}$ $\rho_2 = -4I_{1y}I_{2x}I_{3z}$ $\rho_3 = 4I_{1z}I_{2x}I_{3y}$ $\rho_4 = 2I_{2y}I_{3x}$ $\rho_5 = 2I_{2z}I_{3x}$ $\rho_6 = I_{3y}$ $\rho_7 = -2I_{3x}S_z$ $\rho_8 = 2I_{3z}S_x$ $\rho_9 = -S_y$

$\tau_3 + \tau_2 = 1/(2J_{12})$ $\tau_3 - \tau_2 = 1/(4\Delta\nu_{23})$ $*\tau_4 = 1/(4J_{23})$

Fig. 3 NMR pulse sequence used to perform the relayed polarization transfer depicted in Fig. 2(b). Spin density operators represent each point in time marked by bold numbers assuming J_{13} = 0 and ignoring any relaxation or deviations from the weak-coupling condition. ^{2}H decoupling was used throughout the whole sequence and is not shown. The intervals τ_1 and τ_5 are given by $\tau_1 = 1/(2J_{23})$ and $\tau_5 = 1/(2J_{34})$. The values of the other delays are given in the figure. *In practice, the time interval τ_4 is optimized for the best polarization yield.

 This journal is © The Royal Society of Chemistry 2021

Open Access Article. Published on 15 January 2021. Downloaded on 2/20/2026 8:36:43 PM.
This article is licensed under a Creative Commons Attribution 3.0 Unported Licence.

pyruvate. The *J*-coupling values among the spins were determined from the multiplicity of the spectral lines and are given in the Fig. 2. No special attention was made to the sign of the couplings as they only determine the sign of the spin operator carried over during the sequence resulting in positive or negative polarization at the end of the sequence. With only one ^{13}C to be polarized in the final solution only absolute spin order is considered. The ^{1}H nuclei of the molecules **I** and **II** display chemical shifts that are well separated in the ^{1}H NMR spectrum (Fig. 4). This means all protons fall within the weak coupling regime and as a result the parahydrogen singlet order is effectively projected onto the $2I_{1z}I_{2z}$ spin operator, as in the standard PASADENA experiment.[45,46]

3.2.1. Step 1. Transfer of spin order to the relaying proton. The highly enhanced signals initially observed after hydrogenation reaction can be used to assess the starting spin order. The initial zz-order was estimated by comparing the intensity of the PASADENA pattern with the single NMR line (at 5.50 ppm) of the precursor (Fig. 4(a)). The ratio of signal amplitudes corresponds to 15.5% zz-order, assuming full conversion to molecule **II**. Since the reaction might be incomplete, this figure represents a conservative estimate of the actual polarization degree.

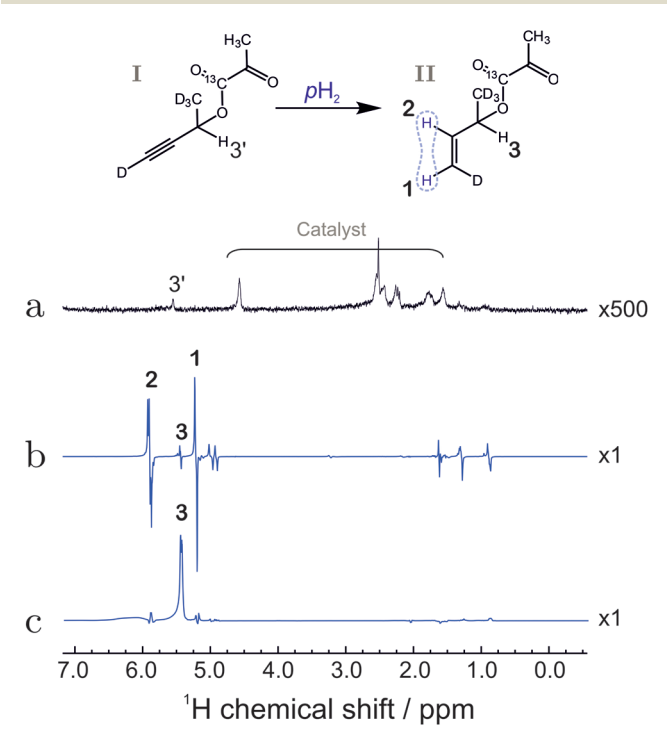

Fig. 4 (a) Spectrum of compound **I** before hydrogenation, recorded by applying a $\pi/2$ pulse to a sample in thermal equilibrium (expanded vertically by a factor of 500). (b) Hyperpolarized ^{1}H spectrum of compound **II**, recorded by applying a $\pi/4$ pulse to the sample after reaction with *para*-enriched hydrogen; (c) ^{1}H spectrum after reaction of substance **I** with *para*-enriched hydrogen, and application of the pulse sequence in Fig. 3 up to time point 6. The spectrum displays the strongly enhanced signal of the relay proton (labelled 3). The bold numbers indicate the spectral lines associated with the protons of interest. For the chemical shifts, see the caption to Fig. 2. The other anti-phase features in the spectrum (b) originate from the fully hydrogenated form of the precursor (signals at 1.3 ppm and 0.9 ppm) as well as a hydrogenated 1,5-cyclooctadiene (signal at 1.6 ppm). The origin of the line at 5 ppm is not fully understood but may be associated with trans-hydrogenation product or impurities.

The zz-order in the sequence (Fig. 3) is converted by a $(\pi/2)_x$ pulse into a $2I_{1y}I_{2y}$ state, which is not directly observable. The J_{23} coupling causes the state to evolve. At the time equal to $1/(2J_{23})$ a pure $4I_{1y}I_{2x}I_{3z}$ is attained if chemical shifts and J_{13} couplings are neglected. The chemical shift, however, is refocused by placement of π_y pulses. Following the same logic, this state would be transformed into a $2I_{2y}I_{3y}$ state using the J_{12} coupling instead.

Here, a slight shift of the π pulse (between point '3' and point '4' in the sequence) plays an important role. Note that the time τ_2 and τ_3 are different. This small difference allows evolution under the chemical shift of the third spin. This leads to a $2I_{2y}I_{3x}$ state at point '4' which allows for the subsequent $(\pi/2)_x$ pulse to generate $2I_{2z}I_{3x}$ spin state.

The sequence efficiency here relies on the obtained spectral resolution and all peaks need to be separated. One reason is that a selective pulse on proton 3 needs to be applied during the transfer. The other is that one part of the sequence relies on the chemical shift difference $\Delta\nu_{23}$ according to $(1/(4\Delta\nu_{23}))$. Overlapping peaks would hence diminish the polarization transfer result.

Having acquired the $2I_{2z}I_{3x}$ state, it gets refocused to the I_{3y} state during the third period (from point '5' to '6') that employs J_{12} coupling the second time. This means that neglecting the remote J_{13} coupling and after three consecutive INEPT blocks (up to point '6') one attains the state which corresponds to observable transverse magnetization.

To test the polarization transfer efficiency up to this point '6', the partial sequence in Fig. 3 was performed after which the ^{1}H NMR signal was collected and Fourier transformed to obtain the NMR spectrum. The spectrum shows that only the relay proton site is significantly polarized (Fig. 4(c)). The calculated enhancement factor of 6405 corresponds to a polarization level of 13.9 ± 1.3%. This corresponds to ~90% of the initial spin order deposited by the hydrogenation reaction. The small loss in polarization is attributed to relaxation losses and to the non-zero J_{13} coupling value which is equal to 1.1 Hz.

3.2.2. Step 2. Magnetization transfer to the heteronucleus. The polarization stored as magnetization of the relay proton is transferred to the ^{13}C of the pyruvate using the last part of the sequence (from point '6' to point '9' in Fig. 3). We have used a standard refocused INEPT sequence employing the J_{34} coupling. However, the carbon-proton coupling (J_{34} = 2.9 Hz) is comparable to the remote proton (J_{13}) coupling. Hence, the magnetization of the third proton is mixed by both couplings on similar timescales. Therefore, the time τ_4 was optimized and set to 350 ms to take into account both scalar couplings yet still magnetizing the ^{13}C site. The optimization was done around the value of 341 ms estimated by the numerical simulation in the supplement. In addition, to fully avoid unwanted spin evolution, a π pulse selective to the relay proton spin was

Open Access Article. Published on 15 January 2021. Downloaded on 2/20/2026 8:36:43 PM.
This article is licensed under a Creative Commons Attribution 3.0 Unported Licence.

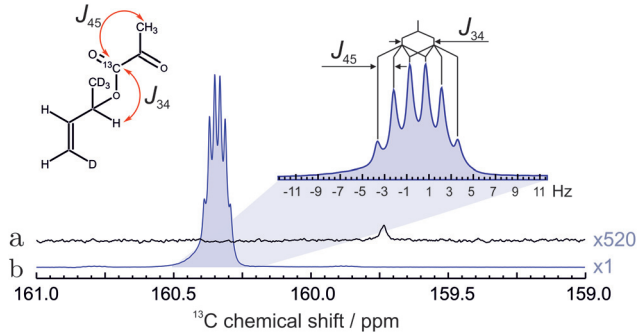

Fig. 5 (a) The spectrum of thermally polarized pyruvate precursor before hydrogenation of the unsaturated side-arm. The spectrum was recorded under ^{1}H decoupling and is multiplied 520 times for clarity. (b) ^{13}C NMR spectrum of the hyperpolarized hydrogenation product collected using the optimized sequence, acquired without ^{1}H decoupling during data acquisition. The expansion shows the multiplet structure due to the indicated ^{13}C–^{1}H *J*-couplings. The polarization level in (b) is estimated to be 7.1%, as determined from the ratio of the spectral intensities in (a) and (b).

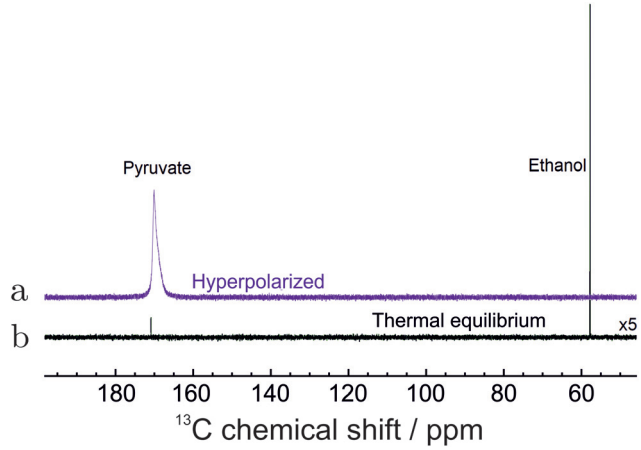

Fig. 6 ^{13}C NMR spectra of hyperpolarized pyruvate in water. (a) The spectrum of hyperpolarized pyruvate dissolved in aqueous solution immediately after all steps in Fig. 2 were concluded. (b) The spectrum recorded with 320 transients after polarization has relaxed to thermal equilibrium at 55 °C. The spectrum is enlarged 5 times for clarity. The ^{13}C polarization level in 1 mM solution is estimated to be 4.33% (see text).

utilized which does not excite the methyl protons. The Gaussian pulse is selective to the relay proton with a chemical shift of 5.44 ppm.

The result of the complete sequence is shown in Fig. 5 and shows the enhanced ^{13}C peak of the ^{13}C pyruvate moiety. The polarization level was estimated to be 7.1 ± 0.4% by comparing the hyperpolarized spectrum with the ^{13}C spectrum recorded before the hydrogenation.

3.3. Cleavage

Before hydrolysis, 400 μL of sodium hydroxide solution was loaded into a syringe which was connected to the NMR tube by a Teflon capillary. After the ^{13}C of the pyruvate derivative was polarized using the PR-SAH routine, the pressure inside the test tube was released and the cleaving solution was injected. The sample was mixed vigorously by nitrogen bubbling. After phases started to separate, the NMR tube was shifted such that only the aqueous phase was positioned within the excitation/detection coil. This was followed by a hard read-out pulse on the ^{13}C channel.

4. Results and discussion

The ^{13}C spectrum of hyperpolarized pyruvate obtained by the total routine (in Fig. 2) is shown in Fig. 6. The increased linewidth of the hyperpolarized spectrum is attributed to magnetic susceptibility changes during injection of the cleavage solution.

The final polarization level was assessed by the following procedure. After the PR-SAH routine was concluded, the sample was allowed to settle at 55 °C temperature. A thermally polarized spectrum was then recorded and compared to the enhanced one. The ^{13}C reference spectrum of the cleaved pyruvate solution was accumulated with 320 repetitions and 2 min relaxation delay using ^{1}H decoupling. Note: the reference spectra of the precursor molecule in Fig. 5 was, however, acquired with 52 transients and 20.3 times increased receiver sensitivity for quicker acquisition. The enhancement factor in Fig. 6 was estimated to be ~8000 which in the corresponding magnetic field of 7.05 T at a temperature of 55 °C translates to 4.33 ± 0.18% polarization.

The concentration of the hydrolysed pyruvate in water was determined to be ~1 mM which is consistent with the dilution caused by addition of water. This value was estimated by comparing the spectral intensity of the thermally polarized sample (Fig. 6(a)) with a reference sample of a well defined concentration using the same experimental conditions.

We would like to underline a few areas for improvement. First, the initial spin order created by the hydrogenation reaction is only a fraction of the full spin order stored in the *para*-enriched gases. The fine adjustments of optimal reaction conditions for rapid and selective hydrogenation could lead to a significantly higher ^{13}C polarization. Separate effort would be also required to yield higher concentration of the (1-^{13}C)pyruvate for future *in vivo* or *in vitro* studies. Second, the hydrolysis step could be automated to reduce the time for extraction and for the overall procedure to respect the relaxation of the hyperpolarized pyruvate. Third, new spin systems with a different set of scalar couplings could be designed to achieve even more effective proton-relay not only limited to pyruvate.

5. Conclusions

We have introduced a side-arm hydrogenation scheme that uses a relaying proton to hyperpolarize a metabolite with a pulsed NMR method. The routine successfully transferred

This journal is © The Royal Society of Chemistry 2021

Open Access Article. Published on 15 January 2021. Downloaded on 2/20/2026 8:36:43 PM.
This article is licensed under a Creative Commons Attribution 3.0 Unported Licence.

spin-order from the side-arm to (1-^{13}C)pyruvate with 46% efficiency which led to 7.6% of ^{13}C polarization. The demonstrated hydrolysis and extraction of the hyperpolarized free pyruvate concluded in 4.3% of ^{13}C polarization. This proves that the proton-relayed SAH method is effective enough to be applied for fast hyperpolarized metabolite delivery.

Conflicts of interest

There are no conflicts to declare.

Acknowledgements

This work was supported by the Marie Skłodowska-Curie program of the European Union (grant number 766402). We acknowledge funding by the Max Planck Society and the German Research Foundation (DFG) grant number DFG418416679. Authors also would like to thank Francesca Reineri and Andreas Trabesinger for their valuable input during the writing process. Open Access funding provided by the Max Planck Society.

References

1 T. Maly, G. T. Debelouchina, V. S. Bajaj, K.-N. Hu, C.-G. Joo, M. L. Mak-Jurkauskas, J. R. Sirigiri, P. C. A. van der Wel, J. Herzfeld, R. J. Temkin and R. G. Griffin, *J. Chem. Phys.*, 2008, **128**, 052211.
2 F. Hill-Casey, A. Sakho, A. Mohammed, M. Rossetto, F. Ahwal, S. B. Duckett, R. O. John, P. M. Richardson, R. Virgo and M. E. Halse, *Molecules*, 2019, **24**, 4126.
3 C. R. Bowers and D. P. Weitekamp, *Phys. Rev. Lett.*, 1986, **57**, 2645–2648.
4 F. D. Colegrove and P. A. Franken, *Phys. Rev.*, 1960, **119**, 680–690.
5 M. Ebert, T. Grossmann, W. Heil, E. Otten, R. Surkau, M. Thelen, M. Leduc, P. Bachert, M. Knopp and L. Schad, *Lancet*, 1996, **347**, 1297–1299.
6 R. W. Adams, J. A. Aguilar, K. D. Atkinson, M. J. Cowley, P. I. Elliott, S. B. Duckett, G. G. Green, I. G. Khazal, J. López-Serrano and D. C. Williamson, *Science*, 2009, **323**, 1708–1711.
7 J. Natterer and J. Bargon, *Prog. Nucl. Magn. Reson. Spectrosc.*, 1997, **31**, 293–315.
8 S. Nelson, D. Vigneron, J. Kurhanewicz, A. Chen, R. Bok and R. Hurd, *Appl. Magn. Reson.*, 2008, **34**, 533–544.
9 K. Münnemann and H. W. Spiess, *Nat. Phys.*, 2011, **7**, 522.
10 R. Weissleder, *Science*, 2006, **312**, 1168–1171.
11 R. Weissleder and U. Mahmood, *Radiology*, 2001, **219**, 316–333.
12 J. W. Gordon, H.-Y. Chen, A. Autry, I. Park, M. Van Criekinge, D. Mammoli, E. Milshteyn, R. Bok, D. Xu, Y. Li, R. Aggarwal, S. Chang, J. B. Slater, M. Ferrone, S. Nelson, J. Kurhanewicz, P. E. Z. Larson and D. B. Vigneron, *Magn. Reson. Med.*, 2019, **81**, 2702–2709.
13 T. Harris, H. Degani and L. Frydman, *NMR Biomed.*, 2013, **26**, 1831–1843.
14 S. J. Nelson, J. Kurhanewicz, D. B. Vigneron, P. E. Z. Larson, A. L. Harzstark, M. Ferrone, M. van Criekinge, J. W. Chang, R. Bok, I. Park, G. Reed, L. Carvajal, E. J. Small, P. Munster, V. K. Weinberg, J. H. Ardenkjaer-Larsen, A. P. Chen, R. E. Hurd, L.-I. Odegardstuen, F. J. Robb, J. Tropp and J. A. Murray, *Sci. Transl. Med.*, 2013, **5**, 1946–6234.
15 K. M. Brindle, *J. Am. Chem. Soc.*, 2015, **137**, 6418–6427.
16 E. Cavallari, C. Carrera, S. Aime and F. Reineri, *Chem. – Eur. J.*, 2017, **23**, 1200–1204.
17 W. Iali, S. S. Roy, B. J. Tickner, F. Ahwal, A. J. Kennerley and S. B. Duckett, *Angew. Chem., Int. Ed.*, 2019, **58**, 10271–10275.
18 M. E. Gemeinhardt, M. N. Limbach, T. R. Gebhardt, C. W. Eriksson, S. L. Eriksson, J. R. Lindale, E. A. Goodson, W. S. Warren, E. Y. Chekmenev and B. M. Goodson, *Angew. Chem.*, 2020, **59**, 418–423.
19 S. S. Roy, K. M. Appleby, E. J. Fear and S. B. Duckett, *J. Phys. Chem. Lett.*, 2018, **9**, 1112–1117.
20 P. J. Rayner, B. J. Tickner, W. Iali, M. Fekete, A. D. Robinson and S. B. Duckett, *Chem. Sci.*, 2019, **10**, 7709–7717.
21 J. Eills, E. Cavallari, C. Carrera, D. Budker, S. Aime and F. Reineri, *J. Am. Chem. Soc.*, 2019, **141**, 20209–20214.
22 B. Ripka, J. Eills, H. Kourilova, M. Leutzsch, M. H. Levitt and K. Muennemann, *Chem. Commun.*, 2018, **54**, 12246–12249.
23 F. A. Gallagher, M. I. Kettunen, S. E. Day, D.-E. Hu, J. H. Ardenkjaer-Larsen, R. in't Zandt, P. R. Jensen, M. Karlsson, K. Golman, M. H. Lerche and K. M. Brindle, *Nature*, 2008, **453**, 940–973.
24 M. Goldman, H. Johannesson, O. Axelsson and M. Karlsson, *C. R. Chim.*, 2006, **9**, 357–363.
25 K. Golman, R. in't Zandt and M. Thaning, *Proc. Natl. Acad. Sci. U. S. A.*, 2006, **103**, 11270–11275.
26 M. Itoda and Y. Naganawa, *RSC Adv.*, 2019, **9**, 18183–18190.
27 K. V. Kovtunov, D. A. Barskiy, R. V. Shchepin, A. M. Co, K. W. Waddell, I. V. Koptyug and E. Y. Chekmenev, *Anal. Chem.*, 2014, **86**, 6192–6196.
28 A. Harthun, K. Woelk, J. Bargon and A. Weigt, *Tetrahedron*, 1995, **51**, 11199–11206.
29 J. Bargon, J. Kandels, P. Kating, A. Thomas and K. Woelk, *Tetrahedron Lett.*, 1990, **31**, 5721–5724.
30 S. Aime, D. Canet, W. Dastru, R. Gobetto, F. Reineri, A. Viale, V. P. Giuria, L. De, H. Poincare, I. Nancy, B. P. Vandoeu and N. Cedex, *J. Phys. Chem. A*, 2001, **105**, 6305–6310.
31 A. S. Kiryutin, K. L. Ivanov, A. V. Yurkovskaya, R. Kaptein and H. M. Vieth, *Z. Phys. Chem.*, 2012, **226**, 1343–1362.
32 R. W. Adams, J. A. Aguilar, K. D. Atkinson, M. J. Cowley, P. I. P. Elliott, S. B. Duckett, G. G. R. Green, I. G. Khazal,

Open Access Article. Published on 15 January 2021. Downloaded on 2/20/2026 8:36:43 PM.
This article is licensed under a Creative Commons Attribution 3.0 Unported Licence.

J. López-Serrano and D. C. Williamson, *Science*, 2009, **323**, 1708–1711.
33 E. Cavallari, C. Carrera, T. Boi, S. Aime and F. Reineri, *J. Phys. Chem. B*, 2015, **119**, 10035–10041.
34 E. Cavallari, C. Carrera, S. Aime and F. Reineri, *J. Magn. Reson*, 2018, **289**, 12–17.
35 F. Reineri, B. Tommasco and S. Aime, *Nat. Commun.*, 2015, **6**, 2041–1723.
36 R. V. Shchepin, D. A. Barskiy, A. M. Coffey, I. V. Manzanera-Esteve and E. Y. Chekmenev, *Angew. Chem., Int. Ed.*, 2016, **55**, 6071–6074.
37 E. Cavallari, C. Carrera, M. Sorge, G. Bonne, A. Muchir, S. Aime and F. Reineri, *Sci. Rep.*, 2018, **8**, 2045–2322.
38 R. V. Shchepin, D. A. Barskiy, A. M. Coffey, I. V. Manzanera Esteve and E. Y. Chekmenev, *Angew. Chem., Int. Ed.*, 2016, **55**, 6071–6074.
39 N. V. Chukanov, O. G. Salnikov, R. V. Shchepin, K. V. Kovtunov, I. V. Koptyug and E. Y. Chekmenev, *ACS Omega*, 2018, **3**, 6673–6682.
40 S. Korchak, S. Yang, S. Mamone and S. Glöggler, *ChemistryOpen*, 2018, **7**, 344–348.
41 S. Korchak, S. Mamone and S. Gloeggler, *ChemistryOpen*, 2018, **7**, 672–676.
42 A. B. Schmidt, S. Berner, M. Braig, M. Zimmermann, J. Hennig, D. von Elverfeldt and J.-B. Hövener, *PLoS One*, 2018, **13**, 1–15.
43 A. B. Schmidt, S. Berner, C. Müller, T. Lickert, N. Schwaderlapp, S. Knecht, J. G. Skinner, A. Dost, P. Rovedo, J. Hennig, D. von Elverfeldt and J. B. Hövener, *Nat. Commun.*, 2017, **8**, 14535.
44 S. Korchak, M. Emondts, S. Mamone, B. Blumich and S. Gloeggler, *Phys. Chem. Chem. Phys.*, 2019, **21**, 22849–22856.
45 O. W. Sørensen, G. W. Eich, M. H. Levitt, G. Bodenhausen and R. R. Ernst, *Prog. Nucl. Magn. Reson. Spectrosc.*, 1984, **16**, 163–192.
46 H. Sengstschmid, R. Freeman, J. Barkemeyer and J. Bargon, *J. Magn. Reson., Ser. A*, 1996, **120**, 249–257.

This journal is © The Royal Society of Chemistry 2021